ELASTIC WAVE SCATTERING BY A SURFACE-BREAKING PLANAR CRACK IN 3d

William M. Visscher

Theoretical Division
Los Alamos National Laboratory
Los Alamos, NM 87545

INTRODUCTION

One of the most important theoretical problems in ultrasonic NDE is the understanding and calculation of scattering of elastic waves from surface flaws, especially cracks, because cracks usually start on, and grow from, surfaces. Cracks can often lead to catastrophic failure, which may be avoided if they can be detected and characterized.

Presented in the present paper is the first theory and computational algorithm with which it is demonstrably possible to calculate the dynamical response of a surface-breaking crack in 3d geometry to an incident elastic wave. The theory has been presented in ref. 1 (referred to in the following as I), and was applied there to the calculation of scattering of SH waves in a 2d geometry from surface-breaking and subsurface cracks. In the present paper (an expanded version[2] will appear in the Journal of Applied Physics) we consider its application to 3d surface-breaking planar cracks normal to the surface of a homogeneous and isotropic half-space.

The method we describe here involves an expansion of the crack-opening-displacements in a set of 3N localized functions on the crack surface. It is expected to be valid for wavelengths large compared with the spacing between localized functions; i.e. $0 < kL \lesssim \sqrt{N}$ for a crack with linear dimension L.

The plan of this paper is to compute the Q and R matrices (see I) with the help of MACSYMA[3] and numerical integration algorithms; then display some results for Rayleigh surface wave scattering from surface-breaking and subsurface cracks of various shapes. A summary and conclusions follow.

COMPUTATION OF THE Q- AND R- MATRICES FOR THE SURFACE CRACK IN 3d

The geometry is envisioned in Fig. 1. An idealized crack (flat, with zero thickness) flaws the homogeneous elastic half-space $z < 0$. The crack can, in principle, have any shape, any orientation or position (including surface-breaking) within the half-space.

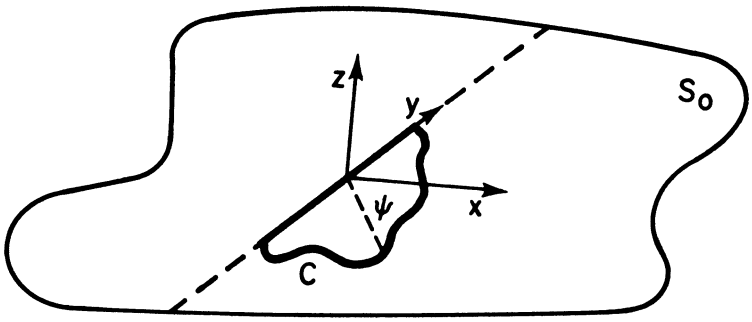

Fig. 1 Geometry of the cracks considered in this paper. S_0 is the infinite plane boundary between the linear isotropic and homogeneous elastic medium which occupies the half-space $z < 0$. The crack C can be buried or can break the xy plane S_0; it lies in a plane which contains the y-axis and makes an angle ψ with the x-axis. For the sake of algebraic simplicity in the present work we take $\psi = 90°$; i.e. C lies in the yz plane.

The crack-opening-displacement (COD) $\Delta u_i(\vec{r})$ (i=x,y,z) is expanded in localized functions $v_n(r)$ as in Eq. I(4.1);

$$\Delta u_i(\vec{r}) = \sum_{n=1}^{N} c_i^n \, v_n(\vec{r}) \quad , \tag{1}$$

where

$$v_n(\vec{r}) = \frac{1}{2\pi\sigma^2} \exp\{-(\vec{r}-\vec{r}_n)^2/2\sigma^2\} \quad , \tag{2}$$

and $\{\vec{r}_n\}$ are chosen on the crack in a square array, as in Fig. 2.

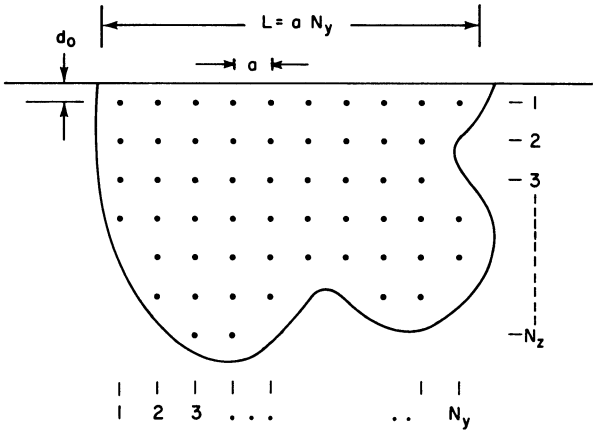

Figure 2. The positions of the centers of the gaussian localized functions are chosen in a square array whose boundaries approximate the crack edges. d_0, the depth of the topmost line of centers needed to simulate a surface-breaking crack, is one of the parameters which must be determined. This crack has $\psi = 90°$; it lies in the yz plane.

Substituting Eq. (1) into the boundary integral representation Eq. I(3.12), multiplying it by $v_m(r)$ and integrating on $d^2r=dS$ yields the matrix equation I(4.3):

$$(Q_{ij}^{mn} - R_{ij}^{mn})\, c_j^n = \tau_i^{om} \quad , \tag{3}$$

where summation on repeated indices is implicit,

$$Q_{ij}^{mn} = \frac{k_s}{\mu} \int dS dS'\; v_n(\vec{r})\; v_m(\vec{r}')\; n_j n_j'\; \Xi_{iji'j'}(\vec{r},\vec{r}') \quad , \tag{4}$$

$$R_{ij}^{mn} = \frac{2ik_s}{\mu} \int d\hat{\gamma}\; \tau_i^{\pi m}(\hat{\gamma}_-) \mathcal{R}_{\pi\pi'}(q)\; \tau_j^{\pi' n\dagger}(\hat{\gamma}_+) \quad , \tag{5}$$

and

$$\tau_i^{\pi m}(\hat{\gamma}) = \int dS\; \tau_i^{\pi}(\hat{\gamma},\vec{r}) v_m(\vec{r}) \quad . \tag{6}$$

In Eqs. (4) and (6) the integrals on dS are over the entire plane in which the crack lies, as discussed in I, and the integral over the complex angle $d\hat{\gamma} = \sin\alpha\, d\alpha\, d\beta$ is on the contour specified in I. The reflection coefficients $\mathcal{R}_{\pi\pi'}(q)$ are given in Eq. I(3.9).

The matrix Q in Eq. (4) has already been calculated.[4] It has the felicitous attribute that it is exactly the matrix which occurs in the isolated planar crack problem, so it can be computed for a crack lying in the xy plane ($\psi = 0°$) and rotated according to Eq. I(4.7) to whatever orientation is needed.

The stress dyadic Ξ which occurs in Q is given by Eq. I(3.2). After it is contracted twice with $\hat{n} = \hat{z}$ (for a crack in the xy plane) it becomes

$$\Xi_{i3i'3}(\vec{r},\vec{r}') = 2i \int_{\bar{C}} d\hat{\gamma}\; t_i^{\pi}(\hat{\gamma},\vec{r})\; t_{i'}^{\pi\dagger}(\hat{\gamma},\vec{r}') \quad , \tag{7}$$

where $t_i^{\pi} = \sigma_{i3}^{\pi}$ are given in Table 1, and $\bar{C}$ is the average of the contours C_+ and C_- (see I(Fig. 2)). In terms of $q = k_\pi \sin\alpha$, $h_\pi = \sqrt{k_\pi^2 - q^2}$ (always positive real or positive imaginary),

$$Q_{ij}^{mn} = \frac{2ik_s}{\mu} \int_0^\infty \frac{q\,dq}{k_\pi h_\pi} \int_0^{2\pi} d\beta\; v_m^{\pi}(\hat{\gamma})\; v_n^{\pi\dagger}(\hat{\gamma})\; t_i^{\pi}(\hat{\gamma})\; t_j^{\pi\dagger}(\hat{\gamma}) \quad , \tag{8}$$

where $t_i^{\pi} = \sigma_{i3}^{\pi}$, the dagger means replace i with -i wherever it explicitly occurs, and

$$t_i^{\pi}(\hat{\gamma},\vec{r}) = t_i^{\pi}(\hat{\gamma})\; e^{ik_\pi \hat{\gamma}\cdot\vec{r}}$$

$$v_m^{\pi}(\hat{\gamma}) = \int_C dS\; e^{ik_\pi \hat{\gamma}\cdot\vec{r}}\; v_m(\vec{r}) = e^{ik_\pi \hat{\gamma}\cdot\vec{r}_m}\; e^{-k_c^2\sigma^2/2} \quad , \tag{9}$$

where $\vec{k}_c$ is the projection of $k_\pi \hat{\gamma}$ on the plane of the crack. As discussed in I, the second equality here follows only if C is extended to include the whole plane of the crack. The sum on π can, given $t_i^\pi(\hat{\gamma})$[2] be carried out, and the integral on β performed, yielding Bessel functions as in Ref. 4.

Similarly, Eq. (5) can be rewritten as

$$R_{ij}^{mn} = \frac{2ik_s}{\mu} \int_0^\infty \frac{q\,dq}{k_\pi h_\pi} \int_0^{2\pi} d\beta\; v_m^\pi(\hat{\gamma}_-)\; \tau_i^\pi(\hat{\gamma}_-)\; \mathcal{R}_{\pi\pi'}(q)\; v_n^{\pi'}(\hat{\gamma}_+)\; \tau_j^{\pi'\dagger}(\hat{\gamma}_+) \quad , \tag{10}$$

where $\mathrm{Im}\,(\cos\alpha_\pm) \gtrless 0$.

The evaluation of R_{ij}^{mn} is considerably more difficult than evaluating Q_{ij}^{mn}, because $R_{\pi\pi'}$ is a 3 x 3 singular matrix function of q, which in (10) is multiplied by two other 3 x 3 matrix functions of q. The matrix product, in general, involves hundreds of terms. To ease the algebraic chores, and to reduce the probability of computational error, we made one simplification; namely, we took $\psi = 90°$, so that our cracks are at right angles to the free surface; and we evaluated the resultant expressions for the integrands of Eqs. (8) and (10) with the help of a computerized symbol manipulation program.[3] The results are given in Ref. 2. (Because of our specialization to $\psi = 90°$, Q and R are block-diagonal; each consists of one N x N plus one 2N x 2N matrix rather than each being a 3N x 3N matrix. They are general complex matrices, neither symmetric nor hermitian.)

The integrals over the angle β in Eqs. (8) and (10) can be straightforwardly done analytically, yielding linear combinations of Bessel functions; for example, in Eq. (10)

$$\frac{1}{2\pi} \int_0^{2\pi} d\beta\; e^{i\xi \sin\beta} \sin^4\beta = \frac{3}{8} J_0 - \frac{1}{2} J_2 + \frac{1}{8} J_4 \quad , \tag{11}$$

where the argument of the Bessel functions is $\xi = q(y_m - y_n)$. Then we are confronted with the main numerical task of the calculation, namely, to perform the integrals over q by some quadrature technique. The integrand of Eq. (10) has three singularities in $0 \le q < \infty$; namely, branch points at $q = k_p$ and k_s, and a pole (which the integration contour should pass below, as discussed in I) at $q = k_R$, the Rayleigh wavenumber, which is, for Poisson's ratio $= \lambda/2(\lambda+\mu) = 1/3$, the value we take for all the numerical work here, $k_R = 1.0723562676808 \ldots\, k_s$. The integral can be efficiently and accurately computed by using Gaussian quadrature schemes.

The parameters upon which Q and R depend are 1) d_0, the burial depth, 2) ω, the angular frequency, 3), Poisson's ratio, and 4) $\{y_n, z_n\}$, the centers of the localized functions. In addition, Q involves σ, the range of the localized functions $v_n(\vec{r})$, and R involves σ', another range parameter introduced to compensate for the unrealistic extension of the crack surface integral.[2]

The set $\{y_n, z_n\}$ is a square array as illustrated in Fig. 2. We will compute matrix elements for a rectangular shape with $N = N_y N_z$ and simulate other shapes by omitting points from the rectangle. d_0 is the depth of the shallowest row; its determination is discussed in Ref. 2.

The optimal localized function range has been determined in Ref. 4 for the isolated crack in 3d to be $\sigma = 0.5a$. This is the same value as that which optimizes the 2d isolated crack (see I). An optimal value of σ' for the 2d in-plane surface-breaking crack problem is found in Ref. 2 to be $\sigma' = 0.1a$. We will adopt this value for the 3d case, also. Other combinations may be better; we have not undertaken a systematic parameter search.

Having computed Q and R for a given frequency (or equivalently, a given $k_s L$) and a given burial depth d_0 on a rectangular square array, we can obtain, from Eq. (3), the COD coefficients c_j^n for incident tractions τ_i^{0m} corresponding to any bulk or surface wave polarization or direction for any shape crack which can be simulated by a subset of the array. From the COD's, in turn, the scattered bulk or surface amplitudes of any polarization and any direction are given by Eqs. I(4.10) and I(4.12), respectively.

The most severe demand on computer time in this work is the numerical integration over q in Eqs. (8) and (10). Not much time is needed; calculating the Q and R matrices takes 15 minutes or less on a CDC 7600 for 25 frequencies and the largest arrays of localized functions we have considered.

NUMERICAL RESULTS

We will concentrate on Rayleigh surface waves in the presentation of results. In general, in the 3d case, an incident wave of any polarization, be it a bulk wave (SH, SV, or P) or a Rayleigh surface wave (R), will produce scattered waves of all 4 varieties.

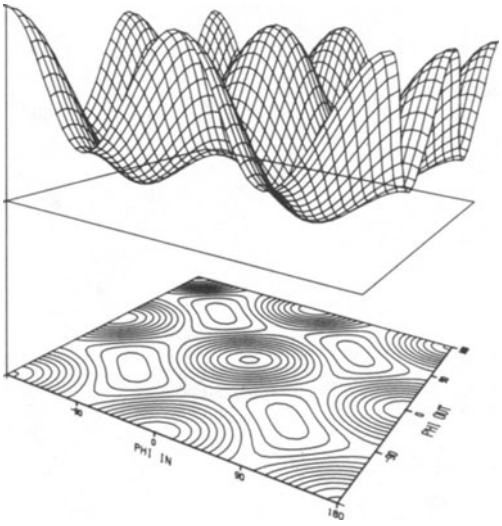

Figure 3. Angular dependence of the modulus of the Rayleigh surface wave scattering amplitude, as a function of azimuths ϕ_{in} and ϕ_{out}, for a square (7 x 7) surface-breaking crack with $k_s L = 0.2$. The dependence of this amplitude on the size and shape and burial depth is describable by just 2 parameters in this long wavelength situation. The shape of this surface for a triangular surface-breaking crack is nearly indistinguishable; it has the same symmetries.

We simulate a surface-breaking crack by a $N_y \times N_z = 7 \times 7$ array of localized functions. Figure 3 shows the angular distribution of the Rayleigh surface-wave scattering amplitude from this rectangular crack for $k_s L = 0.2$. This is in the Rayleigh (long-wavelength) regime, and the angular distribution looks very simple. It is shown in Ref. 2 that, indeed, for any shape crack in this limit this angular distribution is a linear combination of $(\cos^2 \phi_{in} + 1/2)(\cos^2 \phi_{out} + 1/2)$ and $\sin 2\phi_{in} \sin 2\phi_{out}$; hence it is determined by two real parameters describing the size and shape of the crack. The principal perceptible change in Fig. 3 caused by making the crack triangular rather than square is to reduce the maximum amplitude by an amount roughly proportional to the reduction in crack area.

Figure 4 shows the Rayleigh amplitude from a $N_y \times N_z = 9 \times 6$ surface-breaking crack with $k_s L = 8$. This angular distribution manifests the symmetry required by reciprocity ($\phi_{in} \leftrightarrow \phi_{out} + \pi$, see I, Appendix B) plus invariance under ($\phi_{in} \to -\phi_{in}$, $\phi_{out} \to -\phi_{out}$) required by the invariance of the crack shape under $y \to -y$.

Displayed in Fig. 5 is the modulus of the Rayleigh surface wave scattered amplitude for a 9 x 6 triangular crack with $k_s L = 8$. The lack of symmetry under ($\phi_{in} \leftrightarrow \phi_{out}$) is apparent.

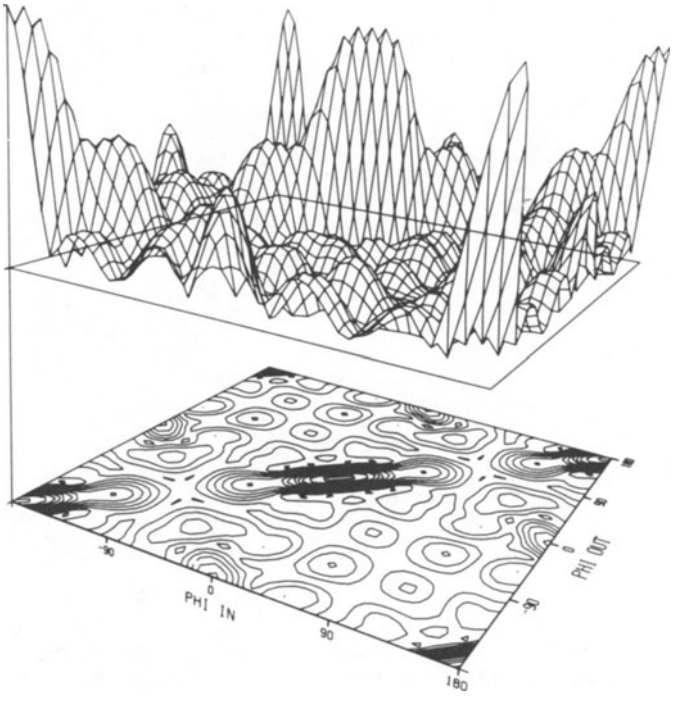

Figure 4. Angular dependence of the modulus of the Rayleigh surface wave scattering amplitude, as a function of azimuths for a rectangular (9 x 6) surface-breaking crack with $k_s L = 8$. This function is symmetric about the main diagonal and the antidiagonal and it has a pronounced ridge along the specular reflection line.

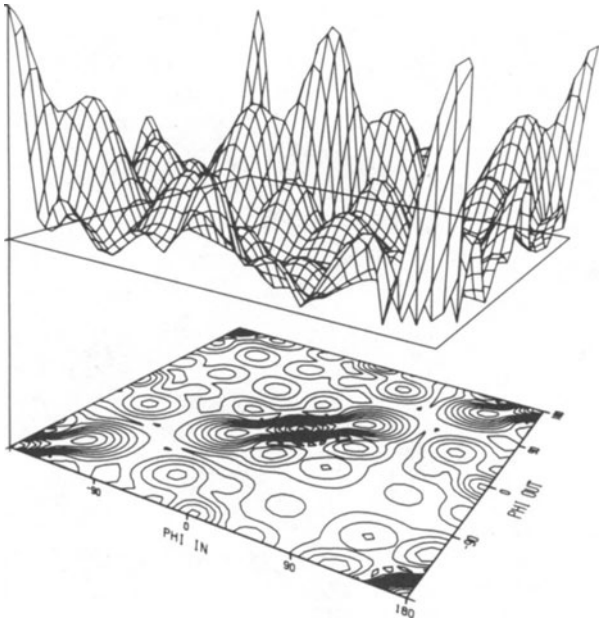

Figure 5. Scattering amplitude at $k_s L = 8$ from a 9 x 6 triangular surface-breaking crack. The specular ridge is pronounced, and symmetry about the main diagonal has disappeared.

Figures 6 and 7 are plots of the modulus of the backscattered Rayleigh surface wave amplitude for rectangular and triangular surface-breaking cracks. Much information about crack size and shape is contained in these data.

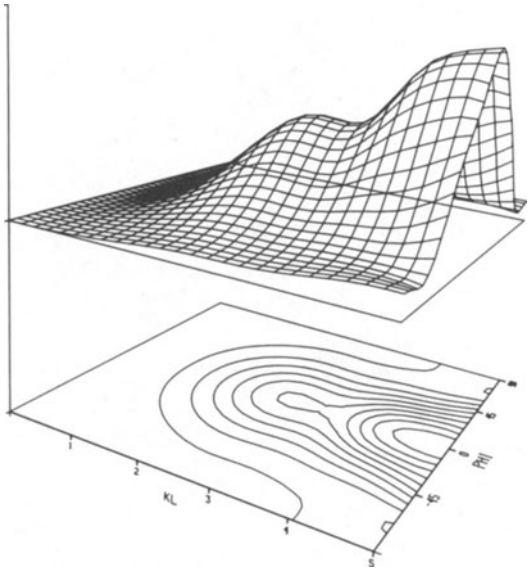

Figure 6. Modulus of the backscattered amplitude from a 12 x 5 rectangle for $0 < k_s L \leq 5$. At low frequencies the amplitude rises like $(k_s L)^{5/2}$.

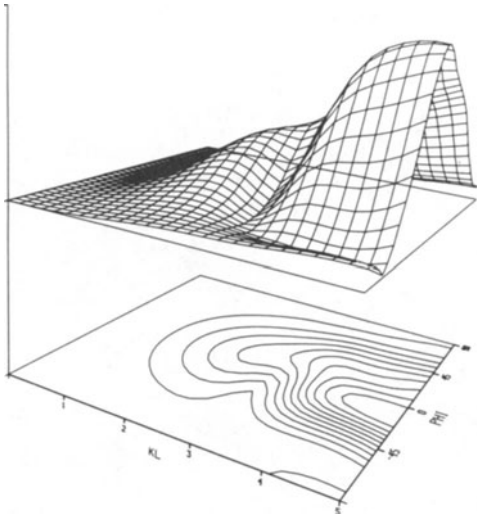

Figure 7. Same as Fig. 6, but for a 9 x 7 triangular crack. The $\phi \rightarrow -\phi$ symmetry has disappeared.

If the crack is buried beneath the surface, then one expects the scattered amplitude to decrease exponentially when the wavelength becomes shorter than the burial depth, on account of the evanescent character of the Rayleigh surface waves. Figure 8 shows the Rayleigh backscattering amplitude from a 7 x 7 crack, buried at a depth about 1.4 times the side of the square. One sees that the amplitude falls off for $kL \gtrsim 3$, as expected.

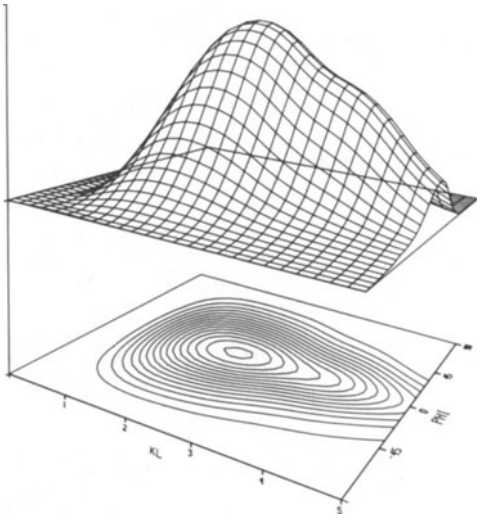

Figure 8. Rayleigh backscattering amplitude for a 7 x 7 triangular crack buried at $d_0 = 10.5a$. As expected, the amplitude decreases rapidly when the wavelength becomes less than the burial depth.

SUMMARY

We have demonstrated the usefulness of the boundary-integral equation method involving expansion in localized functions of the crack-opening-displacement (COD expansion, or CODE) by calculating, for the first time, the dynamics of the scattering of elastic waves from surface cracks of a variety of shapes in 3d for long and intermediate wavelengths. As far as we know, no other methods have been used or are being developed to solve this problem, so the CODE scheme should find wide application in quantitative ultrasonic NDE, because cracks are the most dangerous of defects, and surface cracks are the commonest cracks.

Although onerous, extension of CODE to cracks at angles other than $\psi = 90°$ is straightforward. Computerized manipulative schemes are indispensable, the Q and R-matrices will no longer be block-diagonal, and the matrix elements are more complicated. (An exception, of little practical interest, is the situation when $\psi = 0°$ and the buried crack is parallel to the surface. Then, again, the matrices are block-diagonal.)

REFERENCES

1. William M. Visscher, "Elastic Wave Scattering by a Surface-Breaking or Subsurface Planar Crack," J. App. Phys. August 1, 1984.

2. William M. Visscher, Los Alamos Report LA-UR-84-1956 (Submitted for publication in J. App. Phys.).

3. MACSYMA is a symbolic manipulation program. Symbolics, Inc. 243 Vassar St. Cambridge, MA 02139

4. William M. Visscher, "Elastic Wave Scattering from Flat Cracks," Wave Motion 5 15-32 (1983).